International Journal of Physical Sciences Vol. 7(12), pp. 1884 - 1902, 16 March, 2012
Available online at http://www.academicjournals.org/IJPS
DOI: 10.5897/IJPS12.052
ISSN 1992 - 1950 ©2012 Academic Journals

Full Length Research Paper

High-order balanced *M*-band orthogonal multiwavelet: Construction and application

Hai-jiang Wang[1], Qin-ke Yang[2]* and Chun-mei Wang[1]

[1]Institute of Soil and Water Conservation, Chinese Academy of Sciences and Ministry of Water Resources, Yangling, Shannxi, 712100, China.
[2]Department of Urban and Resource Sciences, Northwest University, Xi'an, 710069, China.

Accepted 17 January, 2012

This article proposed an approach to construct high-order balanced *M*-band (*M*>2) orthogonal multiwavelets with symmetric property, and demonstrated the advantages of our constructed multiwavelet systems in digital elevation model (DEM) generalization application over some other wavelet systems. We studied the theories related to the key properties of *M*-band multiwavelets, such as orthogonality, symmetry, flipping and the particular issue and balancing. According to the theories, we then discussed the construction procedures of the *M*-band multiwavelet systems integrating all the key properties, and presented their realization process based on Gröbner base technique. Three families of orthogonal multiwavelets were achieved in this way, including three-band symmetric family, three-band flipped family and four-band symmetric family. Each family was indexed by a increasingly balanced order ρ ($\rho \in \{1,2,3\}$), and supported with the minimal length according to every balanced order. We finally tested their practical performance in DEM generalization application. The results show the superiority of the constructed *M*-band multiwavelet systems over other widely-used wavelet systems, including multiwavelet of two-band and scalar wavelets of *M*-band and 2-band, and justified the effectiveness of high-order balanced property of these proposed multiwavelet systems in preserving main trend features of signals.

Key words: Multiwavelet, *M*-band, balancing, symmetry, flipping, DEM generalization.

INTRODUCTION

Multiwavelets have some particular advantages over scalar wavelets, mainly shown in the design of finite impulse response (FIR) filter banks (FB) with orthogonal and symmetric properties (Strela et al., 1999; Daubechies, 1992). Since these properties are significant to two-dimensional (2D) signal processing, multiwavelets greatly trigger the interests of researchers. Compared with two-band multiwavelets, *M*-band multiwavelets (*M*>2) offer greater flexibility in choosing time-frequency tiling, and has become a focus of recent studies (Heller and Resnikoff, 1993; Bhatti and Özkaramanli, 2002). However, a crucial problem existed for *M*-band multiwavelets in their design and application just as in the case of two-band and application just as in the case of two-band multiwavelets, that is the approximation power property does not ensure the preservation/cancellation of discrete-time polynomial signals by the lowpass/highpass branch of the FB (Lebrun and Vetterli, 1998, 2001). Mallat (1998) once said the main advantage of wavelets is its approximate ability to practical functions with less nonzero wavelet coefficients. Hence, this problem seriously limits their applications.

Meanwhile, researchers have designed strategies for the problem, such as to intricately preprocess discrete- time data, or to particularly transform multiwavelet basis, but they always destroy certain pretty properties that the multiwavelet basis originally owns, such as symmetry

*Corresponding author. E-mail: qkyang@nwu.edu.cn, wanghaijiang_study@126.com.

ororthogonality, for example (Lebrun and Vetterli, 2001). Besides these, directly constructing specialized balanced multiwavelets is another way for the problem. Fortunately, it also enables a single wavelet system to integrate all the pretty properties above together. By using Gröbner base technique, several families of two-band orthogonal multiwavelets indexed by increasing balanced orders were presented in previous studies (Lebrun and Vetterli, 1998, 2001; Selesnick, 1998, 1999, 2000). However, the related discussion about their *M*-band counterpart is few. Both *M*-band multiwavelet systems and high-order balanced property are very useful in some application. For instance, they are greatly necessary in the application of digital elevation model (DEM) generalization, as an important and well-known requirement in many photogrammetric, remote sensing, and geographic information system application. Wavelet transforms (WT) provide us with an efficient image multiple-level sparse representation approach. Recent studies justified the feasibility of using the WT to generate hierarchically multiple-level-of-detail (LOD) databases from raw DEM data, and obtaining the generalized DEM in different generalized scale by using the WT with different decomposition level (Devarajan et al., 1996; Zhu, 1999; McArthur et al., 2000; Yang et al., 2009). However, it is suggested that integrating the *M*-band multiwavelet systems and high-order balanced property together would improve the performance of this WT based DEM generalization method.

On one hand, *M*-band systems achieve the problem that two-band systems fail to solve in this area; they enable many kinds of generalized scales that the latter could not provide. Using a two-band system, only the generalized scales of 1/2, 1/4, …, $1/2^k$ are accessible (*k* is a positive integer), whereas using an *M*-band system, many other scales beside these will be available, such as 1/3, 1/5, 1/6. In addition, *M*-band multiwavelets lead to less accumulated error resulted from multi-level decompositions compared with the two-band counterparts, since they requires fewer-level decompositions in obtaining the generalized DEM with a specified generalized scale (Zhu, 1999; McArthur et al., 2000; Zhang and Yang, 2005; Lv et al., 2007). As the development of *M*-band wavelets, *M*-band multiwavelets should be introduced into this area. On the other hand, the higher-order balanced property in multiwavelet systems is very necessary in the application of DEM generalization not only because it avoids the oscillations created during the reconstruction from lowpass subband coefficient (or approximate coefficient), but also ensures more smooth features (or trend features) to be preserved by lowpass FB branch (Lebrun and Vetterli, 1998, 2001). Therefore, it is meaningful to integrate high-order balanced property with *M*-band multiwavelet systems that is to directly design the high-order balanced *M*-band multiwavelet systems.

In this study, three families of high-order balanced *M*-band multiwavelets were constructed by using the Gröbner base technique, inspired by the construction scheme of Selesnick (1998, 1999, 2000) and Lebrun (1998, 2001) used in their two-band counterpart construction. The article was organized as follows; the fundamental theories on the key properties of *M*-band multiwavelets were first studied, such as orthogonality, symmetry, flipping and balancing as well. According to the theories and the key instructions for designing *M*-band multiwavelet, we then constructed three families of orthogonal multiwavelets. Every family is of the multiplicity of two, orthogonal and symmetric (or flipped), indexed by an increasing balanced order ρ ($\rho \in \{1,2,3\}$, that is the balanced order of the multiwavelets in each family ranges from one to three), and supported by the minimal length according to each balanced order.

To test the practical performance of these constructed multiwavelet systems, we applied them in the DEM generalization application and analyzed their advantages over other widely-used wavelet systems. Finally, we summarized the results of this study as well as the subsequent tasks in future.

THEORIES ON THE KEY PROPERTIES OF MULTIWAVELETS

An *r*-dimensional (*r*D) column vector function $\Phi_0 = (\phi_{j,0})_{j=1}^{r}$, $1 \le j \le r$ is called a matrix refinable function if;

$$\Phi_0(x) = m\sum_k p_0(k)\Phi_0(mx-k) \quad (1)$$

or equivalently, $\hat{\Phi}_0(w) = P_0\left(w/m\right)\hat{\Phi}_0\left(w/m\right)$. Here and below, $p_0(k)$ is an $r \times r$ real matrix, $P_0 = \sum_k p_0(k)e^{-\sqrt{-1}kw}$, $k, m, r \in \mathbb{Z}$, and $m, r \ge 2$. A compactly support refinable function Φ_0 is called an orthogonal scaling function if the integer shifts $\phi_{j,0}(x-k)$, $1 \le j \le r$ form an orthogonal basis of their closed linear span in $L^2(\mathbb{R})$. A set of *r*D column vector function $\Phi_i = (\phi_{j,i})_{j=1}^{r}$, $1 \le i < m$, defined by

$$\Phi_i(x) = m\sum_k p_i(k)\Phi_0(mx-k), \quad (2)$$

or equivalently, $\hat{\Phi}_i(w) = P_i\left(w/m\right)\hat{\Phi}_0\left(w/m\right)$ for some matrix p_i and matrix filters P_i, is called a set of multiwavelet with the dilation factor m, if its components $\varphi_{j,i}(m^q x-k)$, $1 \le j \le r$, $1 \le i < m$, $q \in \mathbb{Z}$, constitute an orthogonal basis of $L^2(\mathbb{R})$.

Orthogonality

A necessary condition for $\Phi_0(x)$ to be an orthogonal scaling function, or $\Phi_i(x)$, $0 \le i < m$ to be a set of orthogonal multiwavelet is given by Jiang (1998a), that is:

$$\sum_{k=0}^{m-1} P_i(w+2k\pi/m)P_{i'}^*(w+2k\pi/m) = \delta_{i-i'}I_r, 0 \le i, i' < m \quad (3)$$

Here, δ_i is a Dirac sequence; I_r is an $r \times r$ identity matrix, and B^* denotes the Hermitian adjoint of a matrix B. If a set of P_i, $0 \le i < m$, satisfies Equation 3 and belongs to FIR, and $\Phi_0(x)$ defined by Equation (1) is L^2-stable, thus $\Phi_0(x)$ is an orthogonal scaling function, and $\Phi_i, 1 \le i < m$, defined by Equation 2, is a set of multiwavelet function. Under this condition, it is said that P_0 generates an orthogonal scaling function Φ_0, and $\chi = \{P_i, 0 \le i < m\}$ generates a set of orthogonal multiwavelet function $\Phi_i, 1 \le i < m$. Finally, the set χ here is called an *M*-band multiwavelet filter bank.

During the construction of each *M*-band multiwavelet in this study, condition of Equation 3 then would be converted to several particular constrained equations to be added into the equation system, so as to attach orthogonality to the constructed multiwavelet. Different from scalar wavelet, vectorization of input signals is required for multiwavelet. In the case of 1D signal, the input signal should be vectorized to be an *r*D form. Splitting a 1D signal into its polyphase components is a national way to do that, and this is defined as:

$$\begin{bmatrix} y_{0,i}(z) \\ y_{1,i}(z) \\ \vdots \\ y_{r-1,i}(z) \end{bmatrix} = P_i(z) \begin{bmatrix} 1 \\ z^{-1} \\ \vdots \\ z^{-(r-1)} \end{bmatrix}$$

Here, $z = e^{\sqrt{-1}kw}$ and $1 \le i < m$. Then, an *M*-band multiwavelet system can be considered as an $r \times m$ channel filter bank. A crucial problem occurs when the spectral behavior of each component $y_{j,0}(z)$, $0 \le j < r$ is different. In this case, the polyphase method of vectorization will lead to a mixing of the approximate coefficients and detail coefficients, and will finally bring strong oscillations to the result signal reconstructed from the approximate coefficients only (Lebrun and Vetterli, 1998). Therefore, in order to rationally reconstruct the signal from the approximate coefficients, the spectral behavior of $y_{j,0}(z)$ must be same. A balanced *M*-band multiwavelet does this well.

High-order balancing

Balancing

The idea of balancing is to impose some class of smooth signal to be preserved / cancelled by the lowpass / highpass branch. Its definition is as follows; Lebrun and Vetterli (1998) defined L_0 to be the block Toeplitz operator related to lowpass filter branch as shown in Equation 4, and L_i, $1 \le i < m$ to be the block Toeplitz operator related to each highpass filter branch in the same way. Let $v_l = [\cdots (-2)^l \ (-1)^l \ 0^l \ 1^l \ 2^l \cdots]^{\mathrm{T}}$, $l \in \mathbb{N}$ (that v_0 is a constant signal can be seen here).

$$L_0 = \begin{bmatrix} \cdots & & & & & & & & \\ & p_0(0) & p_0(1) & \cdots & p_0(m-1) & p_0(m) & \cdots & & \\ & & & & & p_0(0) & p_0(1) & \cdots & p_0(m-1) & p_0(m) & \cdots \\ & & & & & & & & & & \cdots \end{bmatrix} \quad (4)$$

Definition 1: An orthogonal *M*-band multiwavelet system is said to be balanced (or 1-order balanced) if the lowpass operator L_0^{T} preserves the constant signals, that is $L_0^{\mathrm{T}} v_0 = v_0$.

Theorem 1: The 1-order balancing is equivalent to each condition below (Lebrun and Vetterli, 1998; Mao, 2004; Huang and Cheng, 2006; Yang and Cao, 2006);

① $L_0^{\mathrm{T}} v_0 = v_0$. ② $\sum_{j=0}^{r-1} y_{j,0}(z)$ has $mr-1$ roots in unit circle, that is: $e^{\sqrt{-1}k\pi/m}$, $k = 1, 2, \cdots, mr-1$.

For an orthogonal multiwavelet system, it also means $L_i^{\mathrm{T}} v_0 = 0$, $1 \le i < m$. Hence, a constant signal v_0 can be preserved/cancelled by this lowpass/highpass branch.

High-order balancing

Generally, considering high-order balanced *M*-band multiwavelet systems, it is a natural improvement of the 1-order balanced idea to let higher degree discrete-time polynomial signals to also be preserved by the lowpass branch. Its definition is presented below (Lebrun and Vetterli, 1998);

Definition 2: An orthogonal *M*-band multiwavelet system is said to be *ρ*-order balanced if the lowpass operator L_0^{T} preserves discrete-time polynomial signal of degree *l*, $1 \le l < \rho, \rho \in \mathbb{N}$.

Theorem 2: The *ρ*-order balancing is also equivalent to

each condition below (Lebrun and Vetterli, 1998; Mao, 2004; Yang and Cao, 2006).

$L_0^{\mathrm{T}} v_l = m^{-l} v_l$, $l = 0,1,\cdots,\rho-1$. $\sum_{j=0}^{r-1} U_{j,r}^{(\rho-1)}(z^{mr}) y_{j,0}(z)$ has $mr-1$ roots of order ρ in unit circle, that is $e^{\sqrt{-1}k\pi/m}$, $k = 1,2,\cdots,mr-1$. Here, $U_{j,r}^{(\rho-1)}(z) = u_{j,r}^n(z) \big/ u_{0,r}^n(z)$, and $u_{j,r}^n(z) = \sum_{k\in Z} (kr+i)^n z^{-k}$.

Theorem 2 ① is an approach to verify the balanced order of an orthogonal *M*-band multiwavelet system, and *Theorem* 2 ② is a method to attach high-order balanced property to an *M*-band multiwavelet system. During the construction of the *M*-band multiwavelets in this study, *Theorem* 2 ② was converted to several equations added into the whole equation system for obtaining *ρ*-order balancing, and *Theorem2* ① was applied to verify the result.

Symmetry and flipping property

It is necessary to attach symmetric property to *M*-band multiwavelet systems for its importance in image processing. Therefore, in the first part of this section, we would discuss the theories about a kind of *M*-band multiwavelet system in which every scaling function is symmetric, and every wavelet function is symmetric/ antisymmetric. Next, another kind of *M*-band multiwavelet system, whose scaling functions are flipped with each other and wavelet functions are symmetric/antisymmetric separately, would be studied in the second part because this kind always gain some particular merits at the cost of the symmetry of its scaling functions.

Symmetry

Introduce a vector $C_0 = (c_{1,0},\cdots,c_{r,0}) \in \mathbb{R}^r$ and a matrix;

$$D_0(w) = \begin{bmatrix} \pm e^{-\sqrt{-1}c_{1,0}w/(m-1)} & & \\ & \ddots & \\ & & \pm e^{-\sqrt{-1}c_{r,0}w/(m-1)} \end{bmatrix}$$

Theorem 3: Define $\Phi_0 = (\phi_{j,0},\cdots,\phi_{j,0})^{\mathrm{T}}$ to be a compact support refinable vector with $\hat{\Phi}_0(0) \neq 0$, and P_0 to be its FIR matrix filter, just as the definition above. If P_0 satisfies $D_0(mw)P_0(-w)D_0(-w) = P_0(w)$, then $\phi_{j,0}$ is symmetric/antisymmetric about $c_{j,0}/(2(m-1))$ (Jiang, 2000).

Introduce a vector $C_i = (c_{1,i},\cdots,c_{r,i}) \in \mathbb{R}^r$, $1 \le i < m$, and

$$D_i(w) = \begin{bmatrix} \pm e^{-\sqrt{-1}c_{1,i}w/(m-1)} & & \\ & \ddots & \\ & & \pm e^{-\sqrt{-1}c_{r,i}w/(m-1)} \end{bmatrix}$$

Theorem 4: Define $\Phi_i = (\phi_{j,i},\cdots,\phi_{j,i})^{\mathrm{T}}$ to be a column vector function, and P_i, $1 \le i < m$, to be its FIR matrix filter, as the definition above. Meanwhile, P_0 and Φ_0 meet *Theorem* 3. If P_i satisfies $D_i(mw)P_i(-w)D_0(-w) = P_0(w)$, then $\phi_{j,i}$ is symmetric/antisymmetric about $c_{j,i}/(2(m-1))$ (Jiang, 2000).

Flipping

Flipping provides another kind of symmetry. It focuses on the symmetry among the *r* scaling functions instead of the symmetry within each separate scaling function. In the case of *r* = 2, the two components of the lowpass branch in a *M*-band flipped multiwavelet system, $y_{0,0}(z)$ and $y_{1,0}(z)$, have a clear relationship,

$$y_{1,0}(z) = z^{-2\lambda+1} y_{0,0}(z^{-1}) \tag{5}$$

as presented by Lebrun (1998) and Weidmann (1998). Here, λ is a unique integer related to the maximal polynomial degree between $y_{0,0}(z)$ and $y_{1,0}(z)$. Flipping is not a complete symmetry, although complete symmetric/antisymmetric wavelet functions can be obtained from flipped scaling functions. But at this cost, it brings other advantages such as shorter support length with same smooth level, or higher smooth level with same support length, compared with the completely symmetry discussed above. Likewise, for every constructed symmetric/flipped multiwavelet system below, *Theorem* 3 and Equation (2) was used to add symmetric/flipped property to its scaling functions, and *Theorem* 4 was used to add symmetric (or antisymmetric) property to its wavelet functions.

CONSTRUCTIONS OF MULTIWAVELETS

The WT is always implemented as an iterated digital filter bank tree, so the design of a WT amounts to the design of an FB. The FB designing problem is always achieved by solving a multivariate polynomial system of equations,

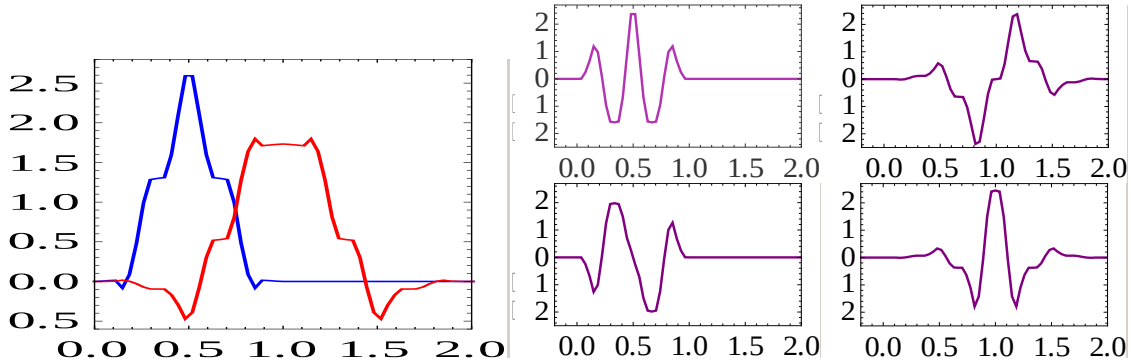

Figure 1. Scaling functions (left) and wavelet functions (right) of 1-order balanced case in family 1.

especially when additional constraints are imposed. Accordingly, the Gröbner base algorithms extend Gaussian elimination to multivariate polynomial systems, and offer an efficient way to obtain solutions, since the equation system is always too complicated to be solved directly. Lebrun (1998, 2001) and Selesnick (1998, 1999, 2000) used Singular software to carry out the Gröbner base computation in designing wavelets and multiwavelet systems, and presented the detailed procedures and complete programs in their homepages. We analyzed the procedures and improved these programs according to the particular properties of *M*-band multiwavelet system, and finally constructed three families of multiwavelets in the similar way. The specific procedures were presented below:

(1) Construct P_0 using fewest free variables at start, whose number is associated with the support length of the scaling functions.
(2) Establish the equation system related to lowpass FB coefficients. With the variables in P_0, convert the condition related to every property (that is ρ-order balancing, orthogonality, symmetry or flipping, respectively) to several particular equations as discussed above, then group them together as an equation system.
(3) Solve the equation system based on the Gröbner bases technique. Increase the numbers of variables (that is to increase the support length) and go back to step (1) when no solution exists (Lebrun and Vetterli, 1998; Buchberger, 2001).
(4) Chose the smoothest from the solutions. In the case that many solutions exist, assess the smoothness of the solutions using an efficient indicator (Sobolev exponent for example, according to study of Jiang in 1998b, is used in this study and abbreviated as *S* below) and select the best. Thus, the lowpass FB coefficients with the properties imposed in step (2) are obtained.
(5) Construct $P_i, 1 \le i < m$, as in step (3).
(6) Establish another equation system related to the high pass FB coefficients. With the variables in P_i, convert the condition related to every property (that is orthogonality, symmetry or flipping) to equations and get an equation system again, like the step (3). Then replace the lowpass variables in these equations with the coefficients obtained in step (4).
(7) Solve the equation system based on the Gröbner base technique again. Finally, the highpass FB coefficients with the properties imposed in step (6) are obtained too.

We also used the Singular software to carry out the Gröbner base computation in this work, and used Maple or Matlab software to calculate the exact or numerical solution from the Gröbner base system. For every multiwavelet system constructed below, only numerical solution was listed out, since few cases (with low ρ) obtained exact solutions due to greatly calculation burden.

Family 1: Three-band symmetric multiwavelets

The three-band multiwavelets, orthogonal and symmetric, with the balanced order ranging from 1 to 3 and the minimal support length for every balance order, were present here.

1-order balanced case

As displayed in Figure 1, the two scaling functions are of lengths (5, 9) (that is the degree of $y_{0,0}(z)$ and $y_{1,0}(z)$ respectively), and are symmetric about (1/2,1) (that is the symmetric place of the two scaling functions, respectively). The *S* exponent is 0.6789.

Among the four wavelet functions displayed in this Figure, the first and the last are symmetric about (1/2,1), while the second and the third are antisymmetric (1/2,1). The solution is presented in Table 1.

Table 1. Coefficients of 1-order balanced case in family 1.

$p_0(0)$ *,$p_0(1)$,$p_0(2)$	0.03867513	0.43301270	0.78867513	0.43301270	0.03867513	0.00000000
	0.00000000	-0.03170907	-0.10566243	0.17604664	0.53867513	0.57735027
$p_0(3)$,$p_0(4)$,$p_1(0)$	0.00000000	0.00000000	0.00000000	0.00000000	0.25149132	-0.53033009
	0.53867513	0.17604664	-0.10566243	-0.03170907	0.00000000	0.03883552
$p_1(1)$,$p_1(2)$,$p_1(3)$	0.55767754	-0.53033009	0.25149132	0.00000000	0.00000000	0.00000000
	0.12940952	-0.21561221	-0.65973961	0.00000000	0.65973961	0.21561221
$p_1(4)$,$p_2(0)$,$p_2(1)$	0.00000000	0.00000000	-0.25444773	0.65973961	0.00000000	-0.65973961
	-0.12940952	-0.03883552	0.00000000	0.02242170	0.07471462	-0.12448377
$p_1(2)$,$p_2(3)$,$p_2(4)$	0.25444773	0.00000000	0.00000000	0.00000000	0.00000000	0.00000000
	-0.38090084	0.81649658	-0.38090084	-0.12448377	0.07471462	0.02242170

*The three symbols here are defined above and now index the following three 2×2 matrixes at the same row respectively.

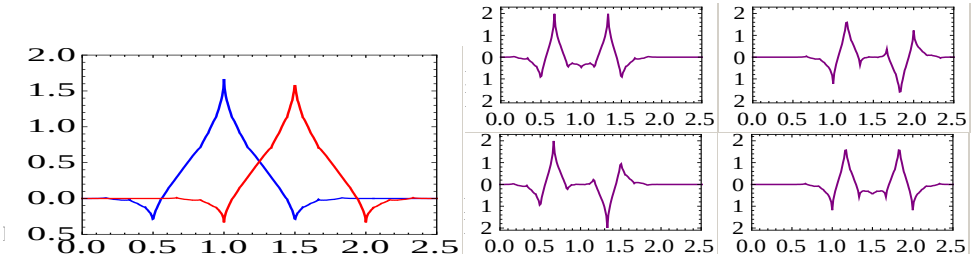

Figure 2. Scaling functions (left) and wavelet functions (right) of 2-order balanced case in family 1.

2-order balanced case

To the 2-order balanced case of this family, the two scaling functions have the same minimal support length of 9, and are symmetric (1,3/2), as seen in Figure 2. Furthermore, the first and the last wavelet functions are symmetric at the two points, and the other two are antisymmetric at the two points, respectively. The *S* exponent for the case is 1.0186, and the solution is given in Table 2.

3-order balanced case

The 3-order balanced case was obtained by increasing the support lengths of the two scaling functions to 17. With the *S* exponent of 1.6886 as shown in Figure 3, they are smoother than the two cases above. The two scaling functions are symmetric about (2,5/2). Similar to the two cases above, two of the wavelet functions are symmetric at these points respectively, and the other two are antisymmetric. The solution is presented in Table 3.

Family 2: Three-band flipped multiwavelets

Also, every one in this family is orthogonal, of ρ-order balancing ($\rho \in \{1,2,3\}$), and with the minimal support length for its balanced order.

1-order balanced case

As shown in Figure 4, the two scaling functions are flipped at 1/2, whereas the four wavelet functions are symmetric/ antisymmetric at the same place. Both support lengths are same as 6, and the *S* is 0.5000. We presented this solution in Table 4.

2-order balanced case

At the place of 5/4, the two scaling functions in this case are flipped, and their four wavelet functions are symmetric/antisymmetric, as seen in Figure 5. The

Table 2. Coefficients of 2-order balanced case in family 1.

$p_0(k),k=0,1,2$	-0.02138334	-0.08553337	0.17106675	0.42766687	0.74841702	0.42766687
	0.00000000	0.00000000	0.00000000	-0.02138334	-0.08553337	0.17106675
$p_0(k),k=3,4,5$	0.17106675	-0.08553337	-0.02138334	0.00000000	0.00000000	0.00000000
	0.42766687	0.74841702	0.42766687	0.17106675	-0.08553337	-0.02138334
$p_1(k),k=0,1,2$	-0.07560154	-0.30240614	0.60481228	-0.12096246	-0.21168430	-0.12096246
	0.00000000	0.00000000	0.00000000	-0.07856742	-0.31426968	0.62853936
$p_1(k),k=3,4,5$	0.60481228	-0.30240614	-0.07560154	0.00000000	0.00000000	0.00000000
	0.00000000	0.00000000	0.00000000	-0.62853936	0.31426968	0.07856742
$p_2(k),k=0,1,2$	-0.07856742	-0.31426968	0.62853936	0.00000000	0.00000000	0.00000000
	0.00000000	0.00000000	0.00000000	-0.07560154	-0.30240614	0.60481228
$p_2(k),k=3,4,5$	-0.62853936	0.31426968	0.07856742	0.00000000	0.00000000	0.00000000
	-0.12096246	-0.21168430	-0.12096246	0.60481228	-0.30240614	-0.07560154

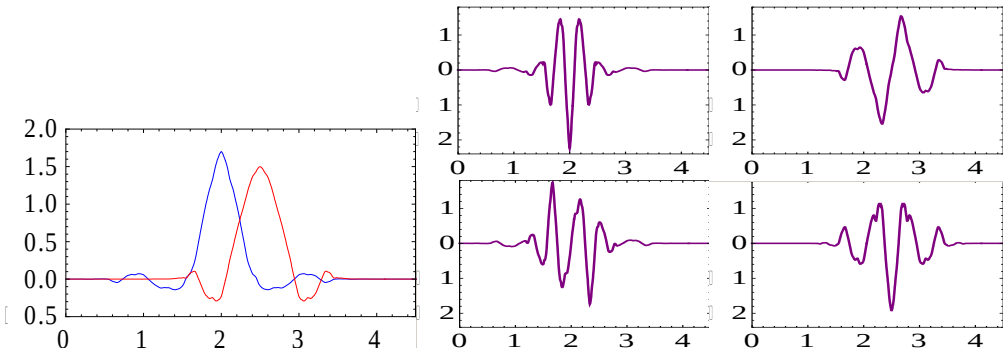

Figure 3. Scaling functions (left) and wavelet functions (right) of 3-order balanced case in family 1.

support lengths are (12,12), the *S* is equal to 1.6462, and the solution is given in Table 5.

3-order balanced case

As displayed in Figure 6, the scaling functions here are flipped at 7/4, and the four wavelet functions are symmetric/antisymmetric at the same place. Compared with the two cases above, the lengths are longer, same as 16, and the smoothness is better, with the *S* of 2.3596. This solution is presented in Table 6.

Family 3: Four-band symmetric multiwavelets

For each balanced order in this family, every pair of scaling functions constructed here are symmetric, but their wavelet functions obtained are antisymmetric. For a pair of scaling functions, 3 pairs of wavelet functions exist here. The rapidly increasing variables and equations make the equation systems so hard to solve, so that some equations related to specified property have to be removed from the equation system in order to find the solution. Hence, the orthogonal wavelet functions without symmetry were obtained.

1-order balanced case

The minimal support lengths of two scaling functions are same as 7, and the symmetric points of the two functions are (1/2,1), as seen in Figure 7. The *S* exponent equals 0.5918, and the solution is presented in Table 7.

Table 3. Coefficients of 3-order balanced case in family 1.

$p_0(0),p_0(1),p_0(2)$	-0.0124966	0.02420801	0.02017305	-0.0366076	-0.0546323	-0.0364798
	0.00000000	0.00000000	0.00000000	0.00073633	0.00142640	0.00911996
$p_0(3),p_0(4),p_1(5)$	0.13077436	0.48189215	0.69838856	0.48189215	0.13077436	-0.0364798
	0.02369307	-0.1023754	-0.0806921	0.20949685	0.48858543	0.63207005
$p_0(6),p_0(7),p_0(8)$	-0.0546323	-0.0366076	0.02017305	0.02420801	-0.0124966	0.00000000
	0.48858543	0.20949685	-0.0806921	-0.1023754	0.02369307	0.00911996
$p_0(9),p_1(0),p_1(1)$	0.00000000	0.00000000	0.01084908	-0.0210164	-0.0175138	0.02392975
	0.00142640	0.00073633	0.00000000	0.00000000	0.00000000	0.00136490
$p_1(2),p_1(3),p_1(4)$	0.03221925	-0.0644634	0.23377684	-0.5027259	0.60988952	-0.5027259
	0.00264403	0.01690458	0.07083686	-0.2419057	-0.1943333	0.24113364
$p_1(5),p_1(6),p_1(7)$	0.23377684	-0.0644634	0.03221925	0.02392975	-0.0175138	-0.0210164
	0.58331659	0.00000000	-0.5833165	-0.2411336	0.19433335	0.24190574
$p_1(8),p_1(9),p_2(0)$	0.01084908	0.00000000	0.00000000	0.00000000	-0.0165489	0.03205803
	-0.0708368	-0.0169045	-0.0026440	-0.0013649	0.00000000	0.00000000
$p_2(1),p_2(2),p_2(3)$	0.02671494	-0.0289012	-0.0344235	0.19342988	-0.5022788	0.45416445
	0.00000000	0.00114924	0.00222627	0.01423345	-0.1388411	0.18081647
$p_2(4),p_2(5),p_2(6)$	0.00000000	-0.4541644	0.50227880	-0.1934298	0.03442350	0.02890128
	0.15633309	-0.3166163	-0.2576100	0.71661812	-0.2576100	-0.3166163
$p_2(7),p_2(8),p_2(9)$	-0.0267149	-0.0320580	0.01654899	0.00000000	0.00000000	0.00000000
	0.15633309	0.18081647	-0.1388411	0.01423345	0.00222627	0.00114924

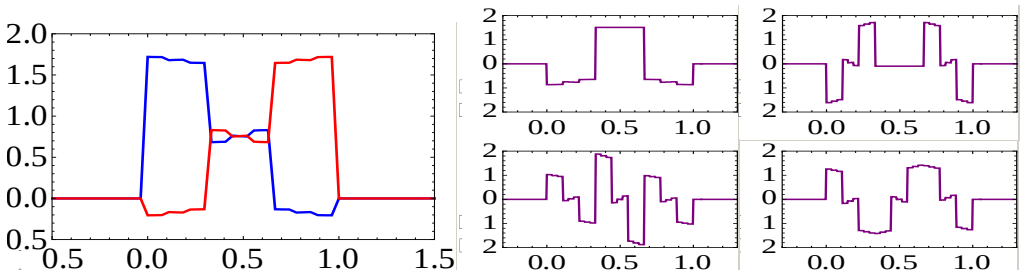

Figure 4. Scaling functions (left) and wavelet functions (right) of 1-order balanced case in family 2.

2-order balanced case

As shown in Figure 8, both scaling functions have the minimal support length of 11, meanwhile, they are symmetric about (1, 3/2). The S is 1.0975, and the solution is given in Table 8.

3-order balanced case

Due to a more complicated equation system compared with all the cases above, the solutions for this case was obtained in a difficult way. As shown in Figure 9, its minimal lengths are (19, 21), and the smoothest has the *S* of 1.4254. The symmetric centers of the two scaling functions are (3/2, 2). We presented this solution in Table 9.

Comparison among the three families

The followings about the two families of three-band (that

Table 4. Coefficients of 1-order balanced case in family 2.

$p_0(k),k=0,1,2$	0.65278390	0.63063138	0.26652261	0.31082766	-0.05328111	-0.07543363
	-0.07543363	-0.05328111	0.31082766	0.26652261	0.63063138	0.65278390
$p_1(k),k=0,1,2$	-0.32088976	-0.25521402	0.57610378	0.57610378	-0.25521402	-0.32088976
	0.37277870	-0.42447770	-0.42527018	0.42527018	0.42447770	-0.37277870
$p_2(k),k=0,1,2$	0.30965409	-0.29317322	0.56406011	-0.56406011	0.29317322	-0.30965409
	-0.47996155	0.51787946	-0.03791791	-0.03791791	0.51787946	-0.47996155

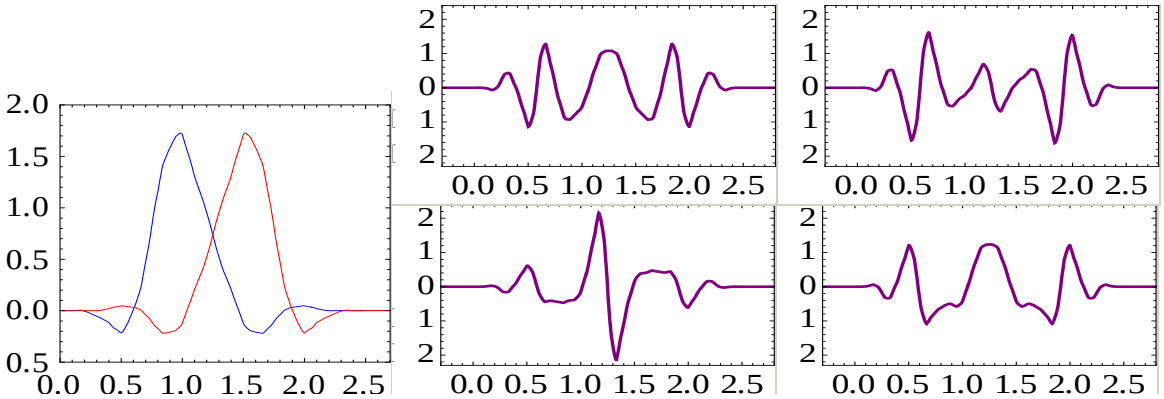

Figure 5. Scaling functions (left) and wavelet functions (right) of 2-order balanced case in family 2.

Table 5. Coefficients of 2-order balanced case in family 2.

$p_0(k),k=0,1,2$	-0.02935033	-0.07539946	0.11656702	0.54599215	0.67456492	0.43552648
	0.00269145	0.01786142	-0.0031086	-0.08210029	-0.0396766	0.16848267
$p_0(k),k=3,4,5$	0.16848267	-0.03967662	-0.0821002	-0.00310861	0.01786142	0.00269145
	0.43552648	0.67456492	0.54599215	0.11656702	-0.0753994	-0.0293503
$p_1(k),k=0,1,2$	0.11112611	-0.32019185	0.36003541	-0.29500579	-0.2091412	0.35317731
	0.12908517	-0.44294091	0.47178362	-0.13492226	-0.0862115	0.19729201
$p_1(k),k=3,4,5$	0.35317731	-0.20914120	-0.2950057	0.36003541	-0.3201918	0.11112611
	-0.19729201	0.08621159	0.13492226	-0.47178362	0.44294091	-0.1290851
$p_2(k),k=0,1,2$	-0.03320796	0.19051291	-0.1377052	-0.18932062	-0.0256215	0.63807568
	-0.07466410	0.36422861	-0.3356214	-0.23805488	-0.1337077	0.41781954
$p_2(k),k=3,4,5$	-0.63807568	0.02562158	0.18932062	0.13770520	-0.1905129	0.03320796
	0.41781954	-0.13370777	-0.2380548	-0.33562141	0.36422861	-0.0746641

Family 1 and 2) can be found; (1) Compared to the symmetric family, the advantages of the flipped family is shown, that is to 2-order balancing, it has the higher *S*, while to 3-order balancing, it has the shorter length as well as the higher *S*. (2) For the two families, the support length and the smoothness both increase as the balanced order rises.

Moreover, for the two families with complete symmetry (Family 1 and 3), the followings can be seen: (1) The higher the balanced order is, the longer the support length

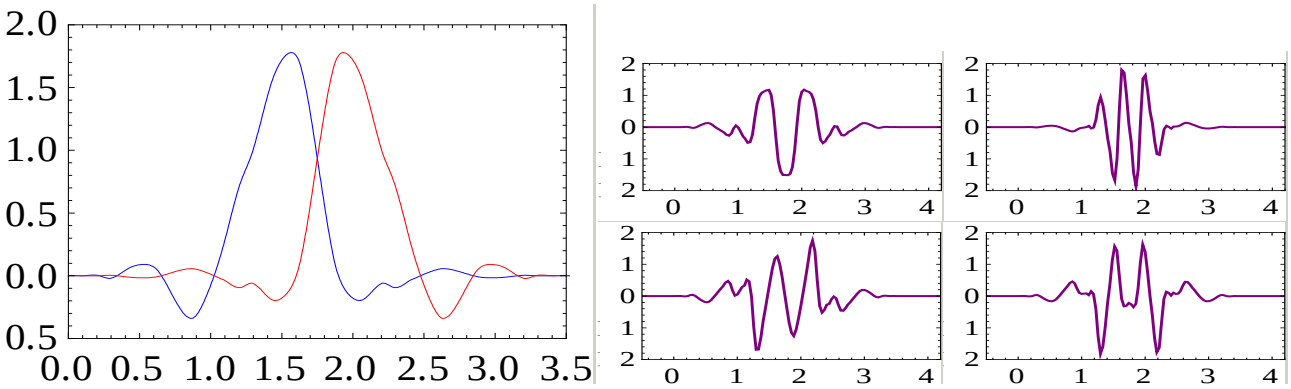

Figure 6. Scaling functions (left) and wavelet functions (right) of 1-order balanced case in family 2.

Table 6. Coefficients of 3-order balanced case in family 2.

$p_0(0)p_0(1),p_0(2)$	0.03439931 -0.00626427	-0.00893307 0.00162675	-0.11981516 0.01990598	-0.03111451 0.00516934	0.21014029 -0.02728008	0.43136001 -0.03686995
$p_0(3),p_0(4),p_1(5)$	0.64594205 -0.07078164	0.55913299 0.12543278	0.12543278 0.55913299	-0.07078164 0.64594205	-0.03686995 0.43136001	-0.02728008 0.21014029
$p_0(6),p_0(7),p_1(0)$	0.00516934 -0.03111451	0.01990598 -0.11981516	0.00162675 -0.00893307	-0.00626427 0.03439931	0.06014722 0.07011644	-0.01561949 -0.01820837
$p_1(1),p_1(2),p_1(3)$	-0.15092729 -0.14970069	-0.03919394 -0.03887541	0.03101509 -0.11457647	0.51988485 0.55100855	-0.44600922 -0.13418676	0.04070278 -0.36889873
$p_1(4),p_1(5),p_1(6)$	0.04070278 0.36889873	-0.44600922 0.13418676	0.51988485 -0.55100855	0.03101509 0.11457647	-0.03919394 0.03887541	-0.15092729 0.14970069
$p_1(7),p_2(0),p_2(1)$	-0.01561949 0.01820837	0.06014722 -0.07011644	-0.01637756 -0.04469703	0.00425305 0.01160726	0.04587948 0.08066135	0.01191433 0.02094675
$p_2(2),p_2(3),p_2(4)$	-0.03591981 0.15786498	-0.21016117 -0.33061507	0.45771976 -0.36696801	-0.49244439 0.47119978	0.49244439 0.47119978	-0.45771976 -0.36696801
$p_2(5),p_2(6),p_2(7)$	0.21016117 -0.33061507	0.03591981 0.15786498	-0.01191433 0.02094675	-0.04587948 0.08066135	-0.00425305 0.01160726	0.01637756 -0.04469703

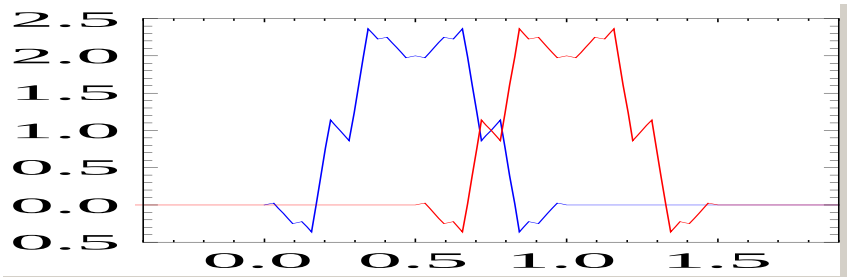

Figure 7. Scaling functions of 1-order balanced case in family 3.

Table 7. Coefficients of 1-order balanced case in family 3.

$p_0(k),k=0,1,2$	-0.05618622	0.25000000	0.55618622	0.50000000	0.55618622	0.25000000
	0.00000000	0.00000000	0.00000000	0.00000000	-0.05618622	0.25000000
$p_0(k),k=3,4,5$	-0.05618622	0.00000000	0.00000000	0.00000000	0.00000000	0.00000000
	0.55618622	0.50000000	0.55618622	0.25000000	-0.05618622	0.00000000
$p_1(k),k=0,1,2$	-0.07841752	0.17708318	0.01167638	0.15397548	-0.42426777	0.43977614
	-0.15495567	0.29177101	-0.23567084	0.12021065	-0.22305823	0.31287882
$p_1(k),k=3,4,5$	0.10911770	-0.33944805	0.09125419	-0.36070294	-0.26116081	0.48111402
	-0.62585870	0.52079752	-0.02415754	0.05074705	0.04107684	-0.07378091
$p_2(k),k=0,1,2$	-0.08803161	0.20760586	0.05231708	0.20074341	-0.06971180	-0.53546958
	0.05418614	-0.13545043	-0.06629784	-0.14781627	0.34536411	-0.26981678
$p_2(k),k=3,4,5$	0.24342685	0.49007453	-0.29703934	-0.36727758	-0.11659822	0.27996041
	-0.41036113	0.03331574	0.55776897	-0.11075276	-0.28304116	0.43290142
$p_3(k),k=0,1,2$	-0.22595926	0.35108925	-0.67459805	-0.06011032	0.51338159	0.12999256
	-0.20618261	0.44519092	-0.06012502	0.34024035	-0.26466040	-0.45527679
$p_3(k),k=3,4,5$	0.23572886	-0.12394280	-0.10054764	-0.06846835	-0.00443860	0.02787277
	-0.02594669	-0.32695591	0.36704979	0.30178934	0.04871827	-0.16384125

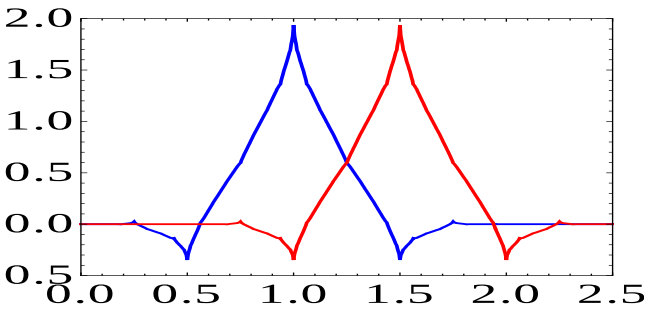

Figure 8. Scaling functions of 2-order balanced case in family 3.

and the smoother the system is. (2) A contradiction exists between the following two sides, one side is the support length and another side is the balanced order as well as the smooth level.

PERFORMANCE IN APPLICATION

DEM generalization belongs to data compression in essence; while the data compression is a key application area for the WT. In order to evaluate the practical performance of the constructed *M*-band multiwavelets, we applied them in DEM generalization application.

For the algorithm of WT based LOD DEM database generalization, as demonstrated in Figure 10, we used a simple generalization algorithm followed that of Zhu (1999), McArthur (2000) and Wu (2001): first to perform a multi-level WT to the original data, and then to perform the inverse WT with all high subband wavelet-domain coefficients zeroed out, while the low subband coefficients kept no changes. That way, one can observe to what extent the method is efficient without the use of more complex generalization algorithm.

With the experiments in this section, we first tested the

Table 8. Coefficients of 2-order balanced case in family 3.

$p_0(0),p_0(1),p_0(2)$	0.00000000	-0.03759203	-0.08106594	0.08740797	0.25000000	0.45018406
	0.00000000	0.00000000	0.00000000	0.00000000	0.00000000	-0.03759203
$p_0(3),p_0(4),p_0(5)$	0.66213187	0.45018406	0.25000000	0.08740797	-0.08106594	-0.03759203
	-0.08106594	0.08740797	0.25000000	0.45018406	0.66213187	0.45018406
$p_0(6),p_0(7),p_1(0)$	0.00000000	0.00000000	0.00000000	0.00000000	-0.02055628	-0.01185112
	0.25000000	0.08740797	-0.08106594	-0.03759203	0.14296382	-0.25211743
$p_1(1),p_1(2),p_1(3)$	-0.06997655	-0.01336025	0.12949384	0.36838902	0.23000544	-0.44941826
	0.26378848	-0.20430870	-0.10566565	0.09997311	-0.24928489	0.19840616
$p_1(4),p_1(5),p_1(6)$	-0.32691694	-0.44187187	0.17333346	0.49840223	0.04629340	-0.03192512
	0.47294058	-0.43257684	-0.17902300	0.21339610	0.34625981	-0.25636991
$p_1(7),p_2(0),p_2(1)$	-0.03440349	-0.04563750	0.18619493	-0.30810719	0.37014408	-0.27634496
	0.02691483	-0.08529645	-0.17820404	0.20431061	-0.38715382	0.12482305
$p_2(2),p_2(3),p_2(4)$	-0.22329864	0.27119560	0.20192979	-0.53116979	0.16753287	0.34294369
	0.35021266	0.27017987	-0.32999347	-0.39388400	0.49663287	0.11296833
$p_2(5),p_2(6),p_2(7)$	-0.01025356	-0.24060304	-0.04774765	0.06125736	0.00517847	0.03114804
	-0.19746299	-0.05268454	-0.00739401	-0.01024349	0.00119249	-0.00329951
$p_3(0),p_3(1),p_3(2)$	0.04794479	-0.06921858	0.09951101	-0.05668782	-0.07425294	-0.04985476
	0.07138057	-0.23912769	0.04478819	-0.17789195	0.24923760	0.54034011
$p_3(3),p_3(4),p_3(5)$	-0.06494215	0.09412137	0.19557575	0.02018473	-0.24895931	0.49971031
	-0.51524879	0.29457834	-0.36987951	0.11304024	0.10946486	-0.12343223
$p_3(6),\ p_3(7)$	-0.68527252	0.35245378	-0.10993600	0.04962234	-	-
	-0.11379884	0.08217632	-0.00050288	0.03487564	-	-

RMSE, Root mean square of error; Max, maximum; Min, minimum; Std, standard deviation.

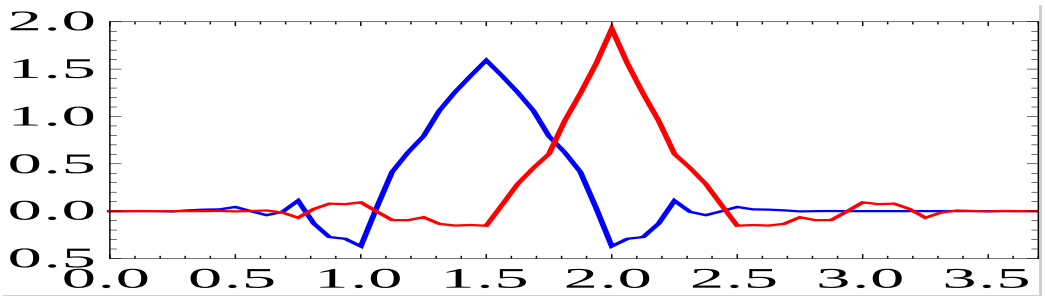

Figure 9. Scaling functions of 3-order balanced case in family 3.

advantages of the proposed *M*-band multiwavelet systems over other widely-used wavelet systems, and then evaluated the effectiveness of high-order balanced property in these multiwavelet systems. Figure 11 displays the original DEM data used in the experiments. The area covered by this DEM is situated in YanHe Basin, Loess Plateau, China. It has a spatial resolution of 5 m, and has a relatively complex terrain so as to gain a deeper study. All the experiments in this section were implemented in Matlab and ArcGIS environments.

Table 9. Coefficients of 3-order balanced case in family 3.

$p_0(k),k=0,1,2$	0.00613368	0.01040717	-0.00882906	0.01257815	-0.09790565	-0.10322554
	0.00000000	0.00000000	0.00000000	-0.01421447	0.02686301	0.02580638
$p_0(k),k=3,4,5$	0.13993715	0.29901870	0.46066388	0.56244303	0.46066388	0.29901870
	-0.02955839	-0.03243474	-0.05644699	-0.04162869	0.09847849	0.23505236
$p_0k),k=6,7,8$	0.13993715	-0.10322554	-0.09790565	0.01257815	-0.00882906	0.01040717
	0.46066388	0.65483831	0.46066388	0.23505236	0.09847849	-0.04162869
$p_0(k),k=9,10,11$	0.00613368	0.00000000	0.00000000	0.00000000	0.00000000	0.00000000
	-0.05644699	-0.03243474	-0.02955839	0.02580638	0.02686301	-0.01421447
$p_1(k),k=0,1,2$	-0.00507810	0.00710181	-0.01935942	0.04917695	-0.04254842	-0.01762121
	0.04051591	-0.06998946	0.17707304	-0.23952936	0.06518977	-0.13612278
$p_1(k),k=3,4,5$	0.01609149	-0.00441760	0.06074225	0.14175608	-0.42625823	0.28280820
	0.11536280	0.16438176	-0.00659978	-0.27868970	-0.05725630	0.28706846
$p_1(k),k=6,7,8$	-0.04562502	0.35563403	-0.41229657	-0.04938046	-0.01894017	0.06373708
	0.26473226	-0.27935334	0.28942177	-0.55932075	0.01415034	0.25774835
$p_1(k),k=9,10,11$	-0.18632926	0.17445261	0.44832319	-0.37087654	-0.00974105	0.00864837
	-0.10656798	-0.02013836	0.16220799	-0.13139715	0.09571695	-0.04860444
$p_2(k),k=0,1,2$	0.00790494	-0.02994372	0.06218494	-0.08675014	0.10262490	0.04361557
	0.00421909	0.00863645	-0.00858057	0.09678407	-0.23604435	-0.23160855
$p_2(k),k=3,4,5$	-0.10627920	-0.24160565	0.46654923	-0.29261344	0.07058849	-0.09853232
	0.29457813	0.44423142	-0.15587671	0.16503185	-0.40850408	-0.35975842
$p_2(k),k=6,7,8$	0.14522218	0.06329775	-0.37104674	0.09372048	0.29307836	0.28588643
	0.30395673	-0.04764542	-0.04637334	0.14560605	0.18862365	0.08705382
$p_2(k),k=9,10,11$	-0.24626305	-0.27202198	-0.11579851	0.09983854	0.26612762	-0.13978469
	-0.13121451	-0.15927459	-0.11303930	0.09522204	0.13569191	-0.07171538
$p_3(k),k=0,1,2$	-0.06476933	0.11561026	-0.28939031	0.48035677	-0.29066549	0.04220370
	0.01875298	-0.02205369	0.06441282	-0.23692976	0.25743375	0.16557629
$p_3(k),k=3,4,5$	0.01624537	-0.02244176	0.01227753	0.02125586	0.20869753	-0.17055466
	-0.15522965	-0.04872922	-0.60664982	0.42092753	0.27459941	-0.07017058
$p_3(k),k=6,7,8$	-0.29670535	0.23742069	0.21937759	-0.41747654	0.10089807	0.25918173
	0.04009557	0.02958624	-0.18699614	-0.09627342	0.14969217	0.21205933
$p_3(k),k=9,10,11$	-0.14145084	-0.10389656	0.05739531	-0.04437259	0.14703631	-0.07623328
	-0.17743833	-0.11759138	0.04342681	-0.03330788	0.15569253	-0.08088557

Advantages of *M*-band multiwavelets over other wavelets

It is the advantage of *M*-band wavelet systems over two-band wavelet systems that fewer-level decompositions bring less accumulated errors, as demonstrated by Zhu (1999) and Zhang (2005). For instance, using a two-band wavelet system, the decomposition of 2*k*-level to an

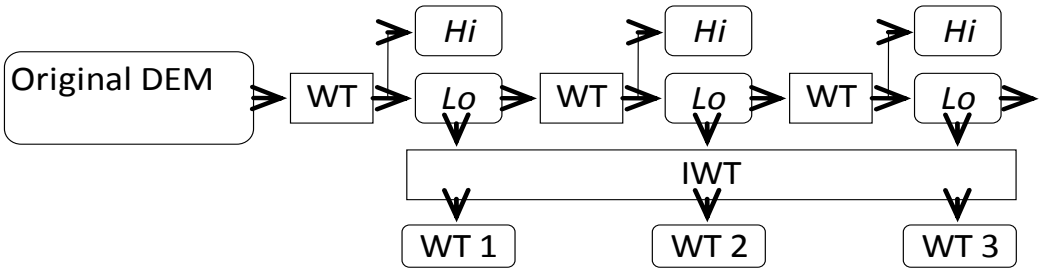

Figure 10. The WT based LOD database generalization algorithm. The Hi and Lo denote the high and low subband coefficients respectively; the IWT denotes the inverse of WT; the WT k denotes the generalized DEM using the WT with k-level decomposition, the same below.

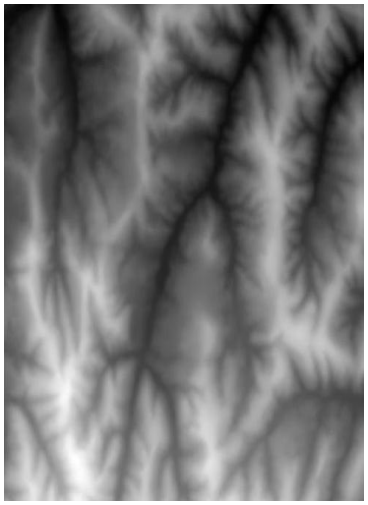

Figure 11. Original DEM data.

original DEM obtains the generalized DEM with the generalized scale of $(1/2)^{2k}$, whereas using a four-band wavelet system, just the decomposition of *k*-level can do this. Thus, the accumulated errors caused by the multi-level decompositions can be reduced, and consequently the deviation between the original and the generalized result can be lessened. In addition, multiwavelets outperform scalar wavelets in FB construction as discussed above. In order to examine the advantages above, we carried out the experiments from two aspects; the assessment to generalized scale and the analysis to generalized deviation for every generalized result. We attempted to finally clarify that for each specified generalized scale, so as to know which one of these systems result in less deviation. For this purpose, only four-band systems and two-band systems were considered in the experiments. It is reasonable to require the compared multiwavelet systems having a same balanced order, so the four-band 3-order balanced case constructed here and the two-band 3-order balanced case designed by Selesnick in 2000 (named symbal3o there) were taken into account in the comparison (abbreviated as four-band MWT and two-band MWT below, respectively). Furthermore, two scalar wavelets of two-band and four-band respectively were also used to evaluate the advantages of multiwavelet. Here, the two-band wavelet known as Daubechies 6 and the four-band wavelet proposed by Steffen and Heller in 1993 (the system with the regularity of 4 in the paper) were chosen for their similar smoothness to other compared systems. Meanwhile, since the Daubechies 6 was also proposed and used by McArthur (2000) in his DEM generalization application, we chose it to make a fair comparison. For simplicity, the two scalar wavelets are denoted as two-band SWT and four-band SWT below respectively.

The generalized scale of each generalized result compared with the original was analyzed in three ways:

(1) At first, it can be approximately assessed by energy ratio *ER* (Wu and Zhu, 2001). Using H^* to represent a generalized DEM, its energy can be calculated by its norm $||H^*||$; using *H* to represent the original DEM, its energy can be calculated by $||H||$. Then, *ER* can be computed via the formula in Equation 6. The similarity between the original and the generalized result is relatively demonstrated by the indicator.

(2) Next, another tool to indirectly assess the generalized scale is gained from length of contours, the ratio *LR*, with the expression in Equation 6. There, *L* and *L** are the total length of the contours derived from the original DEM and the generalized DEM respectively (with a specified contour interval). *LR* can be an indirect indicator to represent generalized scale, because there is a close relationship among length of contours, complexity of terrain, and scale of generalization (Yang et al., 2008). It ranges from zero to one, and is generally closer to zero/one if the generalized scale is higher/lower.

(3) In addition, slope frequency curve, as an effective way to visually display generalized scale, is also used here (Yang et al., 2008). Its horizontal axis represents every slope value, and vertical axis represents the distribution count of every slope value. When generalized scale is higher/lower, more/less flat slopes will be generated from

Table 10. Indicators representing the generalized level of each generalized DEM.

Indicator	Energy		Contour 10*m**		Contour of 20*m*	
	Norm	*ER* (%)	Length (*m*)	*LR* (%)	Length (*m*)	*LR* (%)
Original DEM	907772.9	100.000	643794.9	100.00	333756.7	100.000
2-band SWT 2	907034.9	99.919	639832.3	99.385	329769.6	98.805
2-band MWT 2	906340.4	99.842	641112.2	99.583	330769.2	99.105
4-band SWT 1	906803.4	99.893	641688.4	99.673	331811.9	99.417
4-band MWT 1	906929.6	99.907	642457.7	99.792	332067.9	99.494
2-band SWT 4	900759.4	99.227	571429.1	88.760	284935.1	85.372
2-band MWT 4	901859.7	99.349	573276.8	89.047	289845.0	86.843
2-band SWT 2	901574.6	99.317	569325.2	88.433	284184.5	85.147
4-band MWT 2	900730.4	99.224	567661.0	88.174	287399.9	86.111
2-band SWT 6	890566.1	98.105	458369.1		229237.8	68.684
2-band MWT 6	889492.2	97.986	463793.1		246486.0	73.852
4-band MWT 3	888089.7	97.832	465989.7		234721.4	70.327
4-band MWT 3	889938.8	98.035	461289.3		231312.8	69.306

*Means the total length of contours with the contour interval of 10 m.

generalization, and consequently the main body of the curve will move toward the right/left side.

$$ER = 100 \times \left(|| H^* || / || H || \right)^2 \quad LR = 100 \times L^* / L$$
$$RMSE = \sqrt{\sum_{i=1}^{N} (h_i - h_i^*)^2 / N} \qquad (6)$$

The deviation between the original DEM and every generalized DEM was analyzed based on the following elevation indicators, the middle error, max height, min height, and mean height of the generalized DEM (abbreviated as *RMSE, Max, Min, Mean* below, respectively). The middle error was computed through the formula in (6), where h_i and h_i* represent the cell values of the original and the generalized result respectively.

Discussion on generalize scale of results

The following is shown from Table 10: First, the regular decrease of *ER* along with the rise of the *k* can be seen here. Secondly, we can also find that *LR* decreases regularly as the *k* rises gradually for each case of the contour interval. It is demonstrated by both indicators that the generalized scale regularly increases as the decomposition level rises. Moreover, it is shown from both indicators that the generalized scales obtained from the four-band systems with the decomposition level of *k* are close to those from the two-band systems with the decomposition level of 2*k* (*k*∈1,2,3}).

Figure 12 displays the slope frequency curves derived from the original DEM and several generalized DEMs. The followings are shown: At first, the overall distribution of the slope values is moving towards the left side as *k* is rising in each case of wavelet system. That generalizations bring slope decay into generalized results is obviously displayed here. Next, the two curves related to four-band MWT *k* and two-band MWT 2*k* respectively are approximately distributed (*k*∈{1,2}). This implies their similar generalized scales.

The generalized DEMs obtained from the four-band multiwavelets constructed in this work as well as the original DEM were presented in Figure 13. It is shown that along with the rise of *k*, the local detail features in the original DEM are gradually eliminated, whereas the overall trend features are well retained.

Discussion on generalized deviation of results

The values of the indicators applied to analyze the generalized deviation were presented in Table 11. The followings could be observed: As shown, the *Max* related to every wavelet system decreases, and conversely the *Min* increases as the *k* rises. This demonstrates that the generalized scale increases with the rise in the *k* for every wavelet system. Meanwhile, that the *Mean* varies little in this process indicates the overall trend of the original DEM is well preserved at every decomposition level. Secondly, the decrease of the *Std* along with the rise of the *k* shows the generations gradually cancel the random features of

the original DEM, and the generalized DEM gradually

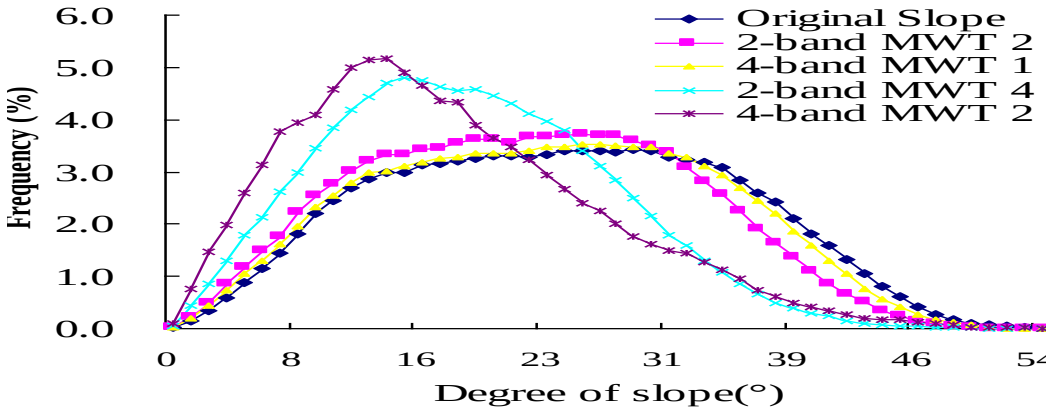

Figure 12. Slope frequency curve resulted from different wavelet systems.

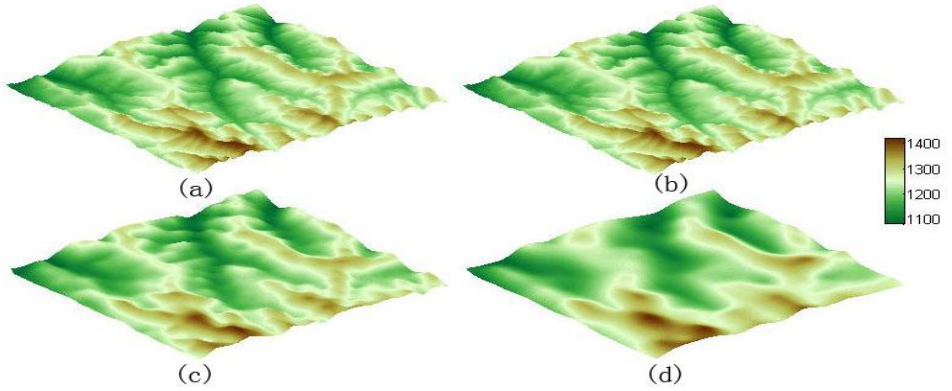

Figure 13. The original DEM (a), and the generalized DEMs (b),(c),(d) resulted from 4-band MWT *k*, *k*=1,2,3 respectively.

Table 11. Elevation indicators of each generalized DEMs.

Indicator	*RMSE*	*Max*(*m*)	*Min*(*m*)	*Mean*(*m*)	*Std*
Original DEM	-	1417.788	1080.396	1231.798	62.746
2-band SWT 2	0.224	1417.709	1080.439	1231.799	62.746
2-band MWT 2	0.219	1417.608	1080.338	1231.794	62.346
4-band SWT 1	0.184	1417.418	1080.532	1231.842	62.582
4-band MWT 1	0.206	1417.692	1080.329	1231.706	62.726
2-band SWT 4	4.925	1413.749	1089.581	1231.789	61.228
2-band MWT 4	5.091	1415.245	1086.397	1231.773	61.530
4-band SWT 2	4.736	1415.441	1087.358	1231.534	61.318
4-band MWT 2	4.235	1412.306	1092.783	1231.489	60.901
2-band SWT 6	23.499	1397.487	1100.722	1231.652	58.774
2-band MWT 6	22.197	1395.248	1102.775	1231.675	58.108
4-band SWT 3	20.422	1400.296	1107.353	1231.668	59.383
4-band MWT 3	19.105	1402.686	1095.641	1231.679	59.207

RMSE, Root mean square of error; Max, maximum; Min, minimum; Std, standard deviation.

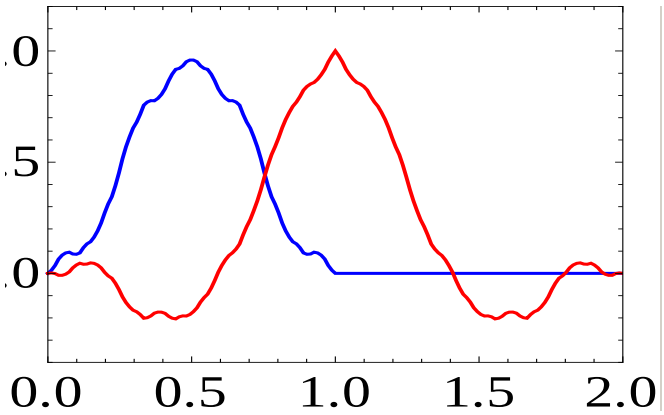

Figure 14. Scale functions of the Asim 3-band multiwavelet.

becomes smooth during the process, just like the display in Figure 13.

In addition, with the discussion on the generalized scale, two facts relating each generalized scale are shown from the indicators *Max*, *Min* and especially *RMSE*. First, the deviations from the four-band wavelet systems are less than those from the two-band systems in most cases, and this phenomenon becomes more obvious as the generalized scale becomes higher. Next, the four-band multiwavelet system always results in less deviation compared with that from the four-band scalar wavelet system. In conclusion, the outperforming of the four-band multiwavelet over the other wavelets (also including the Daubechies 6 wavelet proposed by McArthur, 2000) is shown here.

Effectiveness of high-order balancing

As discussed above, the high-order balanced property of a lowpass/highpass filter branch is the ability to precisely preserve/cancel the trend feature in a signal. The higher balanced order, the more precisely the trend features in a DEM signal can be preserved in approximation coefficient, and the less trend features (or more random features) remain in detail coefficient. This ability can be evaluated by analyzing the spatial self-correlation of the detail coefficient, since the self-correlation will be less significant provided that the coefficient consists of more random features. The Global Moran (*GM*) indicator, as a common approach to calculate the spatial self-correlation of a 2D data, can be used here to gain a quantitative analysis. It was computed via the expression in Equation 7, where $\bar{x}$ is the mean of x_i, and w_{ij} is a weight matrix demonstrating the interaction between x_i and x_j caused by their spatial adjacency. The indicator will be closer to zero if the analyzed signal consists of more random features.

$$GM = N\sum_{i=1}^{N}\sum_{j=1}^{N} w_{ij}\left(x_i-\bar{x}\right)\left(x_j-\bar{x}\right)\Big/\sum_{i=1}^{N}\sum_{j=1}^{N} w_{ij}\sum_{i=1}^{n}\left(x_i-\bar{x}\right)^2 \qquad (7)$$

According to the experimental purpose, the three-band multiwavelets with different balanced order were tested in the experiment. For a general comparison, other two multiwavelets, Alpert three-band multiwavelet and Asim three-band multiwavelet (Alpert, 1993; Bhatti and Özkaramanli, 2002) were considered here, besides the cases constructed above. Both are orthogonal and symmetric, but unbalanced (or 0-order balanced). We applied the particular orthogonal transform of Lebrun (1998) to their basis separately so as to attach balanced property (1-order balancing) to each system.

Unfortunately, just like the discussion above, the symmetry of each system loses at the cost, although the orthogonality still remains. Figures 14 and 15 display the changes of Asim multiwavelet system resulted from the transform.

For each multiwavelet system, $(m^2\text{-}1)r^2$ detail-coefficient parts (m and r are the same as that above) are generated via one-level decomposition to the original DEM. Then the Global Moran indicator of every part is calculated respectively. To obtain a clear comparison, the mean of these indicators was used as a comprehensive Global Moran indicator. Therefore, there is one value for every multiwavelet system to approximately assess how random the information in the detail coefficients is or how precisely the trend feature is preserved in the approximate coefficient. We can see from the Table 12 that for each multiwavelet family, the Global Moran indicator obtained

from their detail coefficient decreases to zero as the ρ rises. This justifies that the ability of the lowpass/highpass filter branch in our constructed multiwavelet systems to precisely preserve/cancel the trend features in a signal is

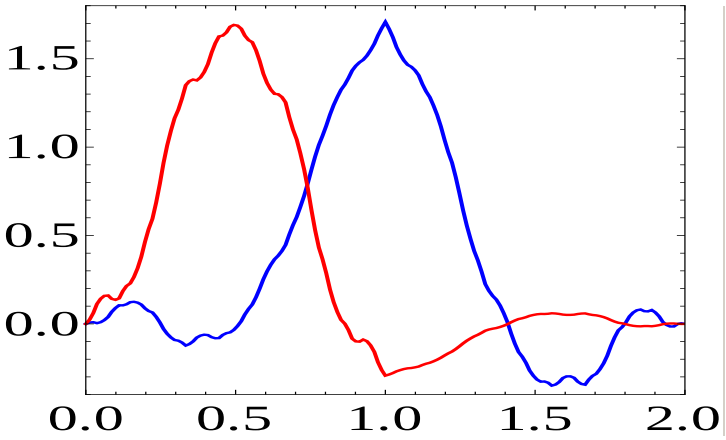

Figure 15. Scale functions of the Asim 1-order balanced 3-band multiwavelet.

Table 12. Global Moran indicators for each multiwavelet

Balanced order ρ		**1**	**2**	**3**
Alpert 3-band 1	0.9224	0.1389	-	-
Asim 3-band 1	0.7916	0.3354	-	-
Symmetric 3-band 1	-	0.1824	0.0780	0.058
Flipping 3-band 1	-	0.2274	0.0776	0.062
Symmetric 4-band 1	-	0.1034	0.0162	0.008

improved as the balanced order rises.

CONCLUSION

For integrating more key properties into a single wavelet system, multiwavelet is proposed after scalar wavelet; for obtaining greater flexibility in choosing the time-frequency tiling, *M*-band multiwavelet is developed following two-band multiwavelet. However, a particular property is very necessary to *M*-band multiwavelet systems, just like the case of two-band multiwavelet systems. After the analysis on the related theories, we presented the procedures of using the Gröbner base technique to construct the *M*-band multiwavelet system that integrates several key properties together, including orthogonality, symmetry, flipping and balancing. Then, we achieved three families of orthogonal multiwavelets in this way, including three-band symmetric multiwavelet, three-band flipped multiwavelet and four-band symmetric multiwavelet. Every family is of the multiplicity of two, indexed by the increasing balanced order ρ ($\rho \in \{1,2,3\}$), and supported by the minimal length according to each balanced order. And for each family, the multiwavelet becomes smoother as the ρ rises. We also tested their practical performances in LOD DEM database generalization application. The results show the advantages of the *M*-band multiwavelets constructed here over other widely-used wavelet systems, including multiwavelet of two-band, scalar wavelets of *M*-band and two-band respectively, and also justified the effectiveness of the high-orders balanced property of the proposed multiwavelets in preserving trend features of signals.

However, the minimal support length of the constructed multiwavelet increases so rapidly as balanced order rises gradually. Hence, other approaches must be put forward subsequently (to raise the multiplicity that is to set the *r* higher). In addition, we should further test the practical performance of the constructed multiwavelets in other signal processing areas in future.

ACKNOWLEDGEMENTS

This research was supported by National Natural Science Foundation of China (Grant Nos.40971173). The authors

would like to thank Ivan W. Selesnick of Polytechnic Institute of New York University and Yang Shouzhi of Department of Mathematics of Shantou University, China, for many useful questions and comments.

REFERENCES

Alpert B (1993). A class of bases in L^2 for the sparse representation of integral operators. SIAM J. Math. Anal., 24: 246-262.

Bhatti A, Özkaramanli H (2002). M-band multiwavelets from spline super functions with approximation order. ICASSP, Orlando, USA. IV-4172.

Buchberger B (2001). Gröbner bases and systems theory. Multidim. Syst. Sign. P. 12: 223-251.

Daubechies I (1992). Ten Lectures on Wavelets. SIAM, Philadelphia USA, pp. 251-312.

Devarajan V, Fuentes R, McArthur DE (1996). An approach to multiple levels of detail generation from digital terrain elevation data using wavelet transforms. 7th Int. Training Equipment Conference Proc. 255-262.

Heller PN, Resnikoff HL (1993). Regular M-band wavelets and applications. ICASSP-93, IEEE Int. Conf. 3: 229-232.

Huang YD, Cheng ZX (2006). Balance for M-Band biorthogonal multiwavelet (in Chinese). J. Xi'an Jiaotong Univ. 40: 1458-1462.

Jiang QT (1998a). On the design of multifilter banks and orthogonal multiwavelets bases. IEEE T. Signal. Proc., 46: 3292-3302.

Jiang QT (1998b). On the regularity of matrix refinable functions. SIAM J. Math. Anal., 29: 1157-1176.

Jiang QT (2000). Parameterization of M-channel orthogonal multifilter banks. Adv. Comput. Math., 12: 189-211.

Lebrun J, Vetterli M (1998). Balanced multiwavelets theory and design. IEEE T. Signal. Proc., 46: 1119-1125.

Lebrun J, Vetterli M (2001). High-order balanced multiwavelets: theory factorization and design. IEEE T. Signal. Proc., 49: 1918-1929.

Lv XK, Yi SR, Han CH (2007). The research of DEM compression based on multi-band wavelet technology (in Chinese). Res. Soil Water Conserv., 14: 125-127.

Mallat S (1998). A Wavelet Tour of Signal Processing. Academic Press, USA, pp. 437-480.

Mao YB (2004). Balance order and interpolatory property of M-band multiwavelets (in Chinese). J. Chongqing Univ., 28: 116-118.

McArthur DE, Fuentes RW, Devarajan V (2000). General of hierarchical multi-resolution terrain database using wavelet filtering. Photogram. Eng. Rem. Sens., 66: 287-295.

Selesnick IW (1998). Multiwavelet bases with extra approximation properties. IEEE T. Signal. Proc., 46: 2998-3021.

Selesnick IW (1999). Balanced GHM-like multiscaling functions. IEEE Signal. Proc. Lett., 6: 111-112.

Selesnick IW (2000). Balanced multiwavelets bases based on symmetric FIR filters. IEEE T. Signal. Proc., 48: 184-191.

Steffen P, Heller PN (1993). Theory of regular M-band wavelet bases. IEEE T. Signal. Proc., 41: 3497-3511.

Strela V, Heller P, Strang P, Heil TC (1999). The application of multiwavelet filter banks to signal and image processing. IEEE T. Image Proc., 8: 548-563.

Weidmann C, Lebrun J, Vetterli M (1998). Significance tree image coding using balanced multiwavelets. P. ICIP, 1: 97-101.

Wu F, Zhu GR (2001). Multi-scaling representation and automatic generalization of relief based on wavelet analysis (in Chinese). Wuhan Univ. Geomatics Info. Sci., 26: 170-174.

Yang QK, David J, Guo WL, Li R (2008). Generalizing the fine resolution DEMs with filtering method (in Chinese). Bull. Soil Water Conserv., 28: 58-62.

Yang QK, Zhao MD, Liu YM, Guo WL, Wang L, Li R (2009). Application of DEMs in regional soil erosion modeling (in Chinese). Geomatics World. 7: 25-31.

Yang, SZ, Cao FL (2006). The balanced orthogonal multiwavelet with a dilation factor of *a* (in Chinese). Prog. Nat. Sci., 12: 177-182.

Zhang LQ, Yang CJ (2005). Real-time massive terrain rendering using M-band wavelet and binary tree (in Chinese). J. Computer-Aided Design Comput. Graphics, 17: 467-472.

Zhu CQ (1999). Application of multi-band wavelet on simplifying DEM with lose of feature information (in Chinese). Acta Geodaetica et Cartographica Sinica. 28: 36-40.